Linker Histones Stabilize the Intrinsic Salt-Dependent Folding of Nucleosomal Arrays: Mechanistic Ramifications for Higher-Order Chromatin Folding†

Lenny M. Carruthers,‡ Jan Bednar,§ Christopher L. Woodcock,§ and Jeffrey C. Hansen*,‡

Department of Biochemistry, The University of Texas Health Science Center at San Antonio, 7703 Floyd Curl Drive, San Antonio, Texas 78284-7760, and Department of Biology, University of Massachusetts, Amherst, Massachusetts 01003

Received July 13, 1998; Revised Manuscript Received August 21, 1998

ABSTRACT: Defined nucleosomal arrays reconstituted from core histone octamers and twelve 208 bp tandem repeats of *Lytechinus* 5S rDNA (208-12 nucleosomal arrays) possess the ability to form an unstable folded species in $MgCl_2$ whose extent of compaction equals that of canonical higher-order 30 nm diameter chromatin structures [Schwarz, P. M., and Hansen, J. C. (1994) *J. Biol. Chem. 269*, 16284−16289]. To address the mechanistic functions of linker histones in chromatin condensation, purified histone H5 has been assembled with 208-12 nucleosomal arrays in 50 mM NaCl. Novel purification procedures subsequently were developed that yielded preparations of 208-12 chromatin model systems in which a majority of the sample contained both one histone octamer per 5S rDNA repeat and one molecule of histone H5 per histone octamer. The integrity of the purified 208-12 chromatin has been extensively characterized under low-salt conditions using analytical ultracentrifugation, quantitative agarose gel electrophoresis, electron cryomicroscopy, and nuclease digestion. Results indicate that histone H5 binding to 208-12 nucleosomal arrays constrains the entering and exiting linker DNA in a way that produces structures that are indistinguishable from native chicken erythrocyte chromatin. Folding experiments performed in NaCl and $MgCl_2$ have shown that H5 binding markedly stabilizes both the intermediate and extensively folded states of nucleosomal arrays without fundamentally altering the intrinsic nucleosomal array folding pathway. These results provide new insight into the mechanism of chromatin folding by demonstrating for the first time that distinctly different macromolecular determinants are required for formation and stabilization of higher-order chromatin structures.

The packaging of DNA in the eukaryotic nucleus involves several distinct hierarchical events (*1*−*5*). The first level of compaction occurs when DNA is wrapped around an octamer of core histones to form a repeating subunit called the nucleosome (*6*−*8*). Histone octamer−DNA complexes are spaced at ∼200 base pair intervals to form nucleosomal arrays, which comprise the central elements of chromatin and chromosomal fibers. Nucleosomal arrays interact with linker histones to form a highly folded transcriptionally repressive "30 nm diameter" chromatin fiber (*3*−*5*, *9*), and with different chromatin-associated proteins to form other types of specific functional chromosomal domains (*4*, *10*). The structure(s) formed by linker histone-containing nucleosomal arrays after they fold into highly condensed "higher-order" 30 nm fibers has long been sought but still remains unsolved (*5*, *6*, *11*, *12*). In contrast, identification of the macromolecular determinants and molecular mechanisms involved in chromatin condensation has progressed more rapidly (*5*, *12*).

For many years, linker histones were believed to be absolutely required for the in vitro formation of highly folded 30 nm chromatin fibers (*3*, *5*, *9*, *13*, *14*). However, characterization of defined model systems reconstituted from core histone octamers and tandemly repeated 5S DNA has revealed that nucleosomal arrays possess the intrinsic ability to form both moderately folded and extensively folded conformational states in the presence of cations (*15*−*19*). The extent of compaction of the extensively folded state is equivalent to that of a highly condensed 30 nm fiber (*17*). Furthermore, it is now well established that higher-order folding of nucleosomal arrays is strictly dependent on the core histone N termini acting through multiple molecular mechanisms (*16*, *18*−*23*). The intermediate and extensively folded conformational states of nucleosomal arrays in and of themselves are not stable (*15*, *17*). Consequently, it has been hypothesized that during formation of the condensed 30 nm fiber, one of the major functions of linker histones is to stabilize the intrinsic folding of nucleosomal arrays (*5*). Implicit in this hypothesis is the idea that incorporation of linker histones will not fundamentally alter the characteristic salt-dependent folding pathway exhibited by nucleosomal arrays in the absence of linker histones.

As the first step in a long-term investigation of the mechanistic roles of linker histones in chromatin condensation, we have developed purification protocols that start with length-defined 5S nucleosomal arrays and yield preparations of histone H5-containing nucleosomal arrays in which a majority of the sample contains both one histone octamer

† This work was supported by NIH Grants GM45916 to J.C.H. and GM43786 to C.L.W.

* Corresponding author. Telephone: (210) 567-6980. Fax: (210) 567-6595. E-mail: hansen@bioc02.uthscsa.edu.

‡ The University of Texas Health Science Center at San Antonio.

§ University of Massachusetts.

10.1021/bi981684e CCC: $15.00
Published on Web 09/25/1998

per 5S rDNA repeat and one molecule of histone H5 per histone octamer. Characterization of these in vitro-assembled chromatin model systems under low-salt conditions by analytical ultracentrifugation, quantitative agarose gel electrophoresis, electron cryomicroscopy, and nuclease digestion together has demonstrated rigorously that binding of histone H5 significantly constrains the entering and exiting linker DNA in a way that produces structures that are indistinguishable from those of native chicken erythrocyte chromatin under low-salt conditions. Results obtained in NaCl and $MgCl_2$ have demonstrated that H5 binding markedly stabilizes both the intermediate and extensively folded states formed by linker histone-deficient nucleosomal arrays at higher salt concentrations. These observations provide new insight into the mechanism of formation of 30 nm fibers by showing that distinctly different macromolecular determinants are required for formation and stabilization of highly condensed chromatin structures. On the basis of these results, we discuss the emerging evidence for the complex functional interplay between linker histones and the core histone N termini during formation of a stably condensed 30 nm fiber.

EXPERIMENTAL PROCEDURES

Materials. Restriction endonucleases were obtained from Promega. Micrococcal nuclease was purchased from Worthington Biochemical. Whole chicken blood was purchased from Pel-Freeze Biologicals. Carboxymethyl-Sephadex C-25 was obtained from Sigma. Low electro-osmosis (LE) agarose was purchased from Research Organics. Spectra/Por 2 dialysis tubing (12000−14000 molecular weight cutoff) was obtained from Spectrum. The 208-12 and 208-6 DNA templates, which contain twelve and six tandem 208 bp repeats of a segment from the *Lytechinus variegatus* 5S rRNA gene, respectively (*24*), were derived from pPOL plasmids (*25*) and purified as described previously (*15*). Core histone octamers were prepared from isolated chicken erythrocyte nuclei and quantitated as described previously (*15*). All reagents used were of analytical grade.

Histone H5 Purification. Histone H5 was fractionated and purified by ion-exchange chromatography as described by Garcia-Ramirez et al. (*26*). The histone H5 concentration was determined using an ϵ_{275} of 0.19 mL mg^{-1} cm^{-1} (*26*). The purity and integrity of histone H5 were confirmed by SDS−polyacrylamide gel electrophoresis. After purification, both histone H5 and the core histone octamers were stored at 4 °C in their respective column elution buffers containing 0.1 mM PMSF, 10 μg/mL aprotinin, and 10 μg/mL leupeptin.

Nucleosomal Array Reconstitution. The 208-12 and 208-6 DNA templates were reconstituted with core histone octamers using the salt dialysis method of Hansen and Lohr (*27*) except that the final DNA concentration was 300 μg/mL and the molar input ratio of histone octamers to 208 bp DNA was 1.3−1.4 rather than 1.1−1.2.

Purification of Saturated Nucleosomal Arrays. Sedimentation velocity analysis in TE buffer [10 mM Tris-HCl, 0.25 mM Na_2EDTA, and 2.5 mM NaCl (pH 7.8)] was used to determine the fraction of reconstituted nucleosomal arrays that were saturated and supersaturated (see Figure 1). After addition of the amount of 208-12 DNA calculated to yield a sample in which all of the DNA templates contained one histone octamer per 208 bp DNA, the mixture was first dialyzed from TE buffer into 2 M NaCl/TE buffer, and subsequently dialyzed back into TE buffer. The extent of template saturation was again determined by sedimentation velocity analysis. These steps were repeated as necessary until the sample contained ∼80% saturated nucleosomal arrays and ∼20% slightly supersaturated arrays. In some cases, it was necessary to add additional core histone octamers to the sample if at some point during these manipulations the 208-12 template contained ≤11 histone octamers per DNA. The Mg^{2+}-dependent oligomerization profile of the sample was next determined as described previously (*17*; see the Figure 5 legend). The nucleosomal arrays were then dialyzed for 2 h against the $MgCl_2$ concentration required to induce oligomerization of the same fraction of the sample that was deemed supersaturated by sedimentation velocity analysis (typically 2.0−3.0 mM), and centrifuged in an Eppendorf microcentrifuge for 30 min at 16000*g* to pellet the oligomers. The supernatant containing the purified nucleosomal array sample was carefully removed and dialyzed against 1 L of TE buffer for 4 h and then dialyzed overnight in 1 L of fresh TE.

Assembly and Purification of Histone H5-Containing Nucleosomal Arrays. Except where otherwise noted, purified preparations of saturated 208-12 nucleosomal arrays were adjusted to 50 mM NaCl and histone H5 was added at ratios (r^{H5}) ranging from 1 to 1.5 mol of H5 per mole of 208 bp DNA repeat. The samples were then mixed, incubated on ice for 3 h, and dialyzed against 1 L of TE buffer for 4 h and then overnight in 1 L of fresh TE. Purification of enriched H5-containing nucleosomal arrays was accomplished using essentially the same procedure described above for nucleosomal arrays except that either $MgCl_2$ or NaCl was used to induce oligomerization of the supersaturated portion of the sample as judged from sedimentation velocity analysis (see the Figure 3 legend).

Analytical Ultracentrifugation. Sedimentation velocity experiments were performed using either a Beckman XL-A or XL-I analytical ultracentrifuge equipped with scanner optics as described previously (*17*). The initial sample absorbance at 260 nm was between 0.6 and 0.8. In all cases, samples were equilibrated at 21 °C in the analytical ultracentrifuge for 1 h prior to sedimentation at 22 000 rpm. Using the Ultrascan data analysis program (version 2.99), the boundaries were analyzed by the method of van Holde and Weischet (*28*) to yield the integral distribution of sedimentation coefficients, plotted as the boundary fraction versus $s_{20,w}$. Except where noted, the entire portion of the boundaries was analyzed. In some cases, the top 10% of the boundaries was omitted from the analysis due to the presence of contaminants (see Figures 6 and 7). Average sedimentation coefficients (s^{ave}) were determined from the rate of sedimentation at the boundary midpoint; i.e., boundary fraction = 0.5 of the sedimentation coefficient distribution plot.

Quantitative Agarose Gel Electrophoresis. Determination of electrophoretic mobilities (μ) of 208-12 nucleosomal arrays and chromatin was accomplished by using 0.2−1.0% agarose multigels as described previously (*29*−*32*). Running gels were cast in E buffer [40 mM Tris-HCl and 0.25 mM EDTA (pH 7.8)] containing either 0 or 0.65 mM free Mg^{2+}. Typically, 208-12 nucleosomal arrays and chromatin samples were electrophoresed on the same gel at 1 V/cm for 8 h and

visualized by UV illumination after ethidium bromide staining. The average gel pore radius (P_e), as well as the gel-free μ (μ_o) and effective radius (R_e) of 208-12 nucleosomal arrays and chromatin, was determined as described previously (*29*−*31*).

Electron Cryomicroscopy. Native chromatin fragments ($N \cong 5-7$) were prepared from long chicken erythrocyte chromatin as described previously (*33*). For electron cryomicroscopy (ECM), a 3 μL drop of specimen adjusted to a concentration of ∼50 μg/mL was applied to an electron microscope grid (covered with platinum-coated perforated supporting film) held in tweezers mounted on a gravity-driven plunger enclosed in a humid chamber (*34*). Excess liquid was blotted with Whatman #52 filter paper, leaving a thin (60−80 nm) film of specimen over the perforations, and the grid plunged into liquid ethane held close to its melting temperature (−180 °C). Without rewarming, the grid was mounted in a model 626-00 (Gatan Inc., Pleasanton, CA) cryo holder and transferred to a Philips CM10 electron microscope equipped with Gatan 651N cryoblade anticontaminator. Stereopair images (30° separation) were recorded at 60 kV at 46000× direct magnification with ∼1 μm underfocus using a low-dose operating mode. Kodak SO163 films were developed in full-strength Kodak D19 developer for 12 min at 22 °C.

For image treatment, the negatives were digitized using a Hamamatsu TV camera with a typical pixel size of 0.53 nm. Image processing was carried out as described previously (*34*). To reduce the underfocus effect, a contrast transfer function (CTF) correction was applied with the amplitude contrast contribution set to 12%, and the images were low-pass filtered using an ideal filter with the cutoff radius set to the position of the first zero of the CTF.

RESULTS

Purification of Saturated 208-12 Nucleosomal Arrays. The 208-12 DNA template used in our studies consists of 12 tandem repeats of a 208 bp portion of the *Lytechinus* 5S rRNA gene (*24*). Depending on the molar histone octamer:DNA input ratio used during reconstitution, it is possible to obtain three distinctly different types of 208-12 nucleosomal arrays. Saturated arrays contain one histone octamer per rDNA repeat, and hence have no octamer-free "gaps". Subsaturated arrays have one or more gaps due to insufficient amounts of added histone octamers. Finally, supersaturated arrays are obtained when the molar histone octamer:DNA input ratio is greater than that required to achieve array saturation; in these cases, the rDNA repeats first become saturated with histone octamers, and then the extra core histone binds nonspecifically to the underlying saturated array through a secondary process that is nonsaturable and eventually produces aggregates (*27*, *35*). Previous work has shown that the degree of histone octamer saturation significantly affects the ability of nucleosomal arrays to undergo both salt-dependent folding and oligomerization. As few as one or two octamer-free gaps abolish the ability of 208-12 nucleosomal arrays to form maximally folded structures (*17*), while at least five gaps abolish folding all together (*30*). Also, relative to saturated arrays, subsaturated and supersaturated arrays oligomerize at higher and lower $MgCl_2$ concentrations, respectively (*36*; see Figure 1). Finally, it has been implied that octamer-free gaps also will affect higher-order folding of linker histone-containing nucleosome arrays (*37*). Therefore, to accurately assess the contributions of histone H5 to the folding and oligomerization of 208-12 nucleosomal arrays, it was first essential to assemble preparations of reconstitutes that to the greatest extent possible consisted of saturated nucleosomal arrays.

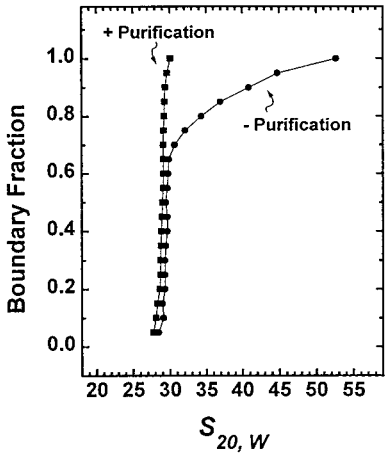

FIGURE 1: Sedimentation velocity analysis of reconstituted 208-12 nucleosomal arrays in TE buffer. Shown are the sedimentation coefficient distribution plots (*28*) obtained before (●) and after (■) array purification as described in Experimental Procedures.

This was achieved by developing an enrichment procedure that allowed us to selectively purify saturated nucleosomal arrays on the basis of the observation that supersaturated arrays oligomerize at lower $MgCl_2$ concentrations than saturated arrays. The first step in this protocol involved purposely supersaturating the 208-12 DNA templates to ensure occupancy of all the rDNA repeats with core histone octamers. Samples subsequently were analyzed by sedimentation velocity analysis in the analytical ultracentrifuge to determine the sedimentation coefficient distribution in TE buffer. Saturated 208-12 nucleosomal arrays in TE buffer sediment at 29−30S (*15*−*17*), while supersaturated arrays sediment at >30S (*27*, *35*, *36*). As judged from the fraction of the initial reconstitutes that sedimented at >30S, the amount of 208-12 DNA estimated to achieve 100% saturation was added to the sample, and the salt dialysis steps were repeated. Figure 1 shows a representative sedimentation coefficient distribution plot of nucleosomal arrays obtained before and after purification by this method. Results indicate that after the initial reconstitution, ∼70% of the sample consisted of saturated nucleosomal arrays while ∼30% was supersaturated. We next determined the $MgCl_2$ concentration necessary to cause oligomerization of ∼35% of the sample, incubated large-scale amounts of arrays at this concentration, pelleted the aggregated material, and dialyzed the supernatant into TE. This resulted in a largely homogeneous sample that sedimented between 27.5S and 30S (Figure 1). These data indicate that 65−75% of the nucleosomal arrays were saturated, with the remaining templates containing 11 histone octamers per 208-12 DNA. In our hands, this is the best result that can be reproducibly obtained without contamination of the sample by supersaturated arrays. To verify the data obtained from the sedimentation analysis, quantitative agarose gel electrophoresis (*29*−*32*) and *Eco*RI digestion (*19*, *20*) assays of the purified nucleosomal arrays were per-

Table 1: Properties of Purified 208-12 Nucleosomal Arrays in Low-Salt Buffers

s^{ave} (S)	R_e (nm)[a]	$-\mu_o$ ($\times 10^{-4}$ cm^2 V^{-1} s^{-1})	% free DNA[b]
29	28.1 ± 1.1	1.82 ± 0.04	2.8 ± 0.3

[a] Value represents the mean ± standard deviation of 18 determinations at $P_e \geq 200$ nm (see Experimental Procedures). [b] Value represents the mean ± standard deviation of the percentage of unoccupied 5S rDNA determined by the *Eco*RI digestion assay (*19*).

formed. Quantitative electrophoresis of length-defined nucleosomal arrays in low-percentage agarose multigels yields the effective radius (R_e) and gel-free mobility (μ_o), both of which provide sensitive measures of the average level of array saturation (*29*−*31*). The R_e and μ_o values of the purified 208-12 nucleosomal array sample (Table 1) were within 5% of the values reported previously for preparations of predominantly saturated nucleosomal arrays (*29*). Each 5S rDNA repeat of the 208-12 DNA template is flanked by *Eco*RI sites (*24*). The amount of histone octamer-free 5S rDNA repeats liberated by *Eco*RI digestion of the purified arrays (Table 1) indicated that the sample was ~70% saturated with histone octamers (see refs *19* and *20*). Together, the results shown in Figure 1 and Table 1 demonstrate that the selective purification protocol yielded highly enriched preparations of saturated 208-12 nucleosomal arrays.

Histone H5 Binding to Purified 208-12 Nucleosomal Arrays. Several methodologies exist for assembling linker histones onto nucleosomal arrays. One method involves adding linker histone at the 0.3−0.6 M NaCl step in the dialysis protocol. While this approach yields viable reconstitutes (*38*, *39*; see Figure 4C), it is very difficult to accurately control both the histone octamer and linker histones stoichiometries of the final reconstituted product. Consequently, we chose to add histone H5 to purified preparations of 208-12 nucleosomal arrays at NaCl concentrations ranging from 0 to 50 mM. This general approach previously has been used to successfully reconstitute linker histone onto both mononucleosomes (*40*−*42*) and endogenous, mixed-length nucleosomal arrays (*37*, *43*−*48*). Addition of histone H5 to 208-12 nucleosomal arrays in TE produced mostly large aggregates, and there was no evidence of stoichiometric H5 binding (data not shown). However, as will be documented below, when H5 was added to purified 208-12 nucleosomal arrays in 50 mM NaCl, we were able to obtain linker histone-containing nucleosomal arrays that both exhibited native morphology under low-salt conditions and dramatically stabilized folding behavior in NaCl and $MgCl_2$. Note that the terms "linker histone-containing nucleosomal arrays" and "chromatin" will be used interchangeably throughout the remainder of the paper.

Initially, histone H5 was added to purified 208-12 nucleosomal arrays in 50 mM NaCl using molar H5:208 bp repeat ratios (r^{H5}) of 1.0−1.5. Subsequent analysis on native 1.2% agarose gels (Figure 2A) revealed that H5 binding led to several distinct phenomena. Incubation with increasing amounts of H5 caused a reduction in mobility of the 208-12 chromatin "monomer", eventually producing a discrete slower migrating chromatin band at $r^{H5} = 1.5$. Smearing between the 208-12 nucleosomal array and chromatin bands was observed at $r^{H5} = 1.0-1.4$, suggesting that some of the

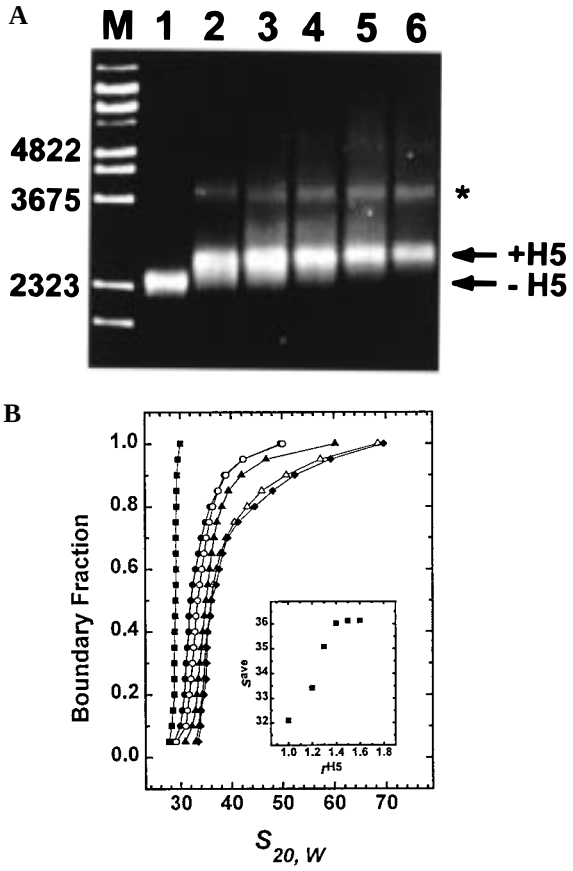

FIGURE 2: Binding of histone H5 to purified 208-12 nucleosomal arrays. (A) Native agarose gel electrophoresis. One microgram of purified 208-12 nucleosomal arrays incubated with histone H5 at r^{H5} values of 0, 1.0, 1.2, 1.3, 1.4, and 1.5 (lanes 1−6, respectively) was electrophoresed for 4 h at 2 V/cm in a 1.2% agarose gel buffered with 40 mM Tris-acetate and 1 mM EDTA (pH 8.0), and bands were visualized by staining in ethidium bromide. Arrows indicate the discrete bands formed by 208-12 nucleosomal arrays (−H5) and 208-12 chromatin (+H5). Aggregated chromatin dimers are indicated by the asterisk. Lambda DNA digested with *Bst*EII was used as size markers (lane M). (B) Sedimentation velocity analysis. Shown are the sedimentation coefficient distribution plots in TE for purified 208-12 nucleosomal arrays incubated at r^{H5} values of 0 (■), 1.0 (●), 1.2 (○), 1.3 (▲), 1.4 (△), and 1.5 (◆). The inset indicates the average sedimentation coefficient (s^{ave}) as a function of r^{H5}.

208-12 chromatin contained substoichiometric amounts of H5 at these ratios. In addition, both a dimeric chromatin species and a smearing between the monomer and dimer chromatin bands were present at all r^{H5} values examined (Figure 2A). More extensively aggregated material also was observed at the higher r^{H5}. Similar effects of H5 on aggregation of chicken erythrocyte nucleosomal arrays have been described previously (*37*, *48*).

To characterize the H5 binding process quantitatively, we next examined the various 208-12 chromatin samples by sedimentation velocity and quantitative electrophoresis in agarose multigels. Figure 2B shows the sedimentation coefficient distribution plots of purified 208-12 nucleosomal arrays after incubation with increasing amounts of histone H5 in 50 mM NaCl and dialysis into TE prior to sedimentation. These data both confirm and extend the results of the gel experiment. With increasing r^{H5} values, the average sedimentation coefficient of 208-12 nucleosomal arrays first increased and then reached a plateau at 35S (Figure 2B inset).

Table 2: Electrophoretic Properties of H5-Containing 208-12 Nucleosomal Arrays in Low-Salt Buffer

r^{H5}	R_e (nm)[a]	$-\mu_o$ ($\times 10^{-4}$ cm^2 V^{-1} s^{-1})
1.0	26.3 ± 1.1	1.72 ± 0.1
1.2	24.6 ± 0.9	1.60 ± 0.1
1.3	23.5 ± 1.3	1.55 ± 0.1
1.4	21.3 ± 1.0	1.52 ± 0.09
1.5	21.2 ± 0.9	1.52 ± 0.07

[a] Values represent the mean ± standard deviation of six to eight determinations at $P_e \geq 200$ nm.

At $r^{H5} = 1.0$, the sedimentation coefficient distribution of the unaggregated chromatin fraction ranged from 29S to 35S, but became increasingly more homogeneous as r^{H5} approached 1.5 (Figure 2B). By $r^{H5} = 1.5$, ~50% of the sample sedimented at 35S, ~15% sedimented at <35S, and the remainder consisted of rapidly sedimenting H5-induced aggregates. These data indicate that the discrete gel band observed at $r^{H5} = 1.5$ (Figure 2A) sediments at 35S in TE buffer. The sedimentation distribution profiles further showed that both the total fraction of the chromatin samples that sedimented at >35S and the average and maximum sedimentation coefficients of this fraction increased as the r^{H5} increased from 1 to 1.5. Thus, like histone octamer assembly onto 208-12 DNA, addition of greater than stoichiometric amounts of H5 to 208-12 nucleosomal arrays led to formation of H5-supersaturated oligomers (Figure 2A).

The 35S chromatin species identified above was further characterized by quantitative agarose gel electrophoresis to determine the R_e and μ_o. The R_e value for nonspherical molecules such as chromatin correlates with the surface area of a rod, and changes significantly in response to the alterations in conformation that occur during both assembly (*29*) and salt-dependent folding of nucleosomal arrays (*18*, *19*, *30*). The μ_o value also is a sensitive indicator of both nucleosomal array composition and conformation (*18*, *20*, *29*, *30*). Both the R_e and μ_o exhibited saturable behavior with increasing r^{H5} values (Table 2), as was observed in the native gel and sedimentation velocity experiments (Figure 2A,B). The decrease in R_e that occurs upon H5 binding indicates that 208-12 chromatin is more compact than the parent nucleosomal arrays under low-salt conditions. The difference in the μ_o values of saturated 208-12 nucleosomal arrays and chromatin is equivalent to a gain of 75 ± 3 positive charges per rDNA repeat. Chicken erythrocyte H5 has a net positive charge of ~62 as determined from its amino acid sequence (*49*, *50*). Thus, the histone H5 stoichiometry of the 35S chromatin species is ~1.0−1.2 H5 per nucleosome, which is essentially identical to the linker histone stoichiometry of native chicken erythrocyte chromatin (*51*). Given a stoichiometry of ~1 H5 per rDNA repeat, the >20% increase in sedimentation coefficient caused by H5 binding (Figure 2B) cannot be explained solely by the ~9% calculated increase in array mass. Thus, both the hydrodynamic and electrophoretic analyses indicate that H5 binding leads to a small but significant global compaction of the nucleosomal array in TE buffer.

Histone H5 Constrains the Entering and Exiting Linker DNA of Purified 208-12 Chromatin. To test for the constraint of entering and exiting linker DNA, as well as to generate preparations of 208-12 chromatin that are suitable for folding studies, it was first necessary to purify the

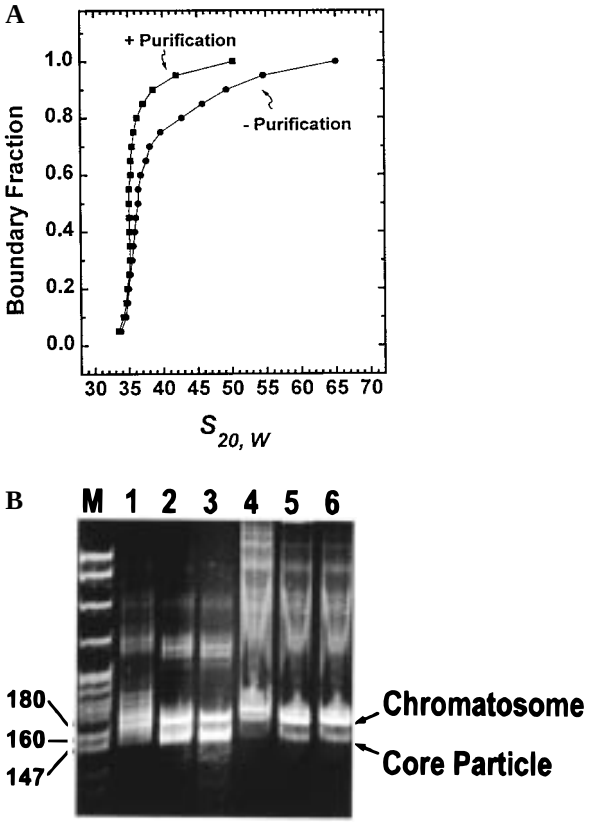

FIGURE 3: Purification of 208-12 chromatin. (A) Sedimentation velocity analysis. 208-12 chromatin assembled at $r^{H5} = 1.5$ was purified using the same procedure described for nucleosomal arrays in Experimental Procedures except that either $MgCl_2$ or NaCl (typically ~1.3 mM $MgCl_2$ or ~130 mM NaCl) was used to induce oligomerization of the supersaturated portion of the sample. Shown are the sedimentation coefficient distribution plots in TE buffer of the chromatin sample at $r^{H5} = 1.5$ before (●) and after (■) purification. (B) Micrococcal nuclease digestion. Purified 208-12 nucleosomal arrays (lanes 1−3) and chromatin (lanes 4−6) were digested with 0.05 unit of micrococcal nuclease per microgram of DNA in the presence of 0.5 mM $CaCl_2$. The DNA concentration was 60−80 μg/mL. The products obtained after digestion for 0.5, 1, or 2 min at 22 °C are shown from left to right for each sample. The reactions were quenched and histones dissociated by addition of $^1/_5$ volume of a solution containing 0.1 M EDTA, 5% SDS, 25% glycerol, and 0.3% bromophenol blue. Samples were electrophoresed for 2 h at 20 mA in a 5% polyacrylamide gel buffered with 40 mM Tris-acetate and 1 mM EDTA (pH 8.0) and bands visualized by staining in ethidium bromide. *Msp*I-digested pBR322 DNA was used as size markers (lane M).

saturated 35S chromatin from the contaminating supersaturated chromatin. Much like in the enrichment process for nucleosomal arrays (Figure 1), we exploited the fact that supersaturated 208-12 chromatin oligomerizes at lower salt concentrations than saturated chromatin. Representative sedimentation coefficient distributions in TE of 208-12 chromatin before and after purification are shown in Figure 3A. These data yield two key observations. First, the purification procedure reduced the amount of supersaturated arrays from ~50% to only ~10% of the sample. Second, ~70% of the enriched sample sedimented at 35S to 36S, while 20% sedimented between 33S and 35S. The R_e and μ_o of the purified chromatin sample as determined by quantitative agarose gel electrophoresis were 21.0 ± 1.0 nm and -1.52×10^{-4} cm^2 V^{-1} s^{-1}, respectively. These values are the same as those listed in Table 2, indicating that the properties of the enriched 208-12 chromatin were not altered

by the purification process. Together, these results demonstrate that ~70% of the purified 208-12 chromatin contained stoichiometric amounts of both histone octamers and histone H5. In contrast, the fraction of the sample that sedimented between 33S and 34S consisted of arrays having mostly 11−12 histone octamers per 208-12 DNA template and slightly less than one H5 per nucleosome.

The most common assay for determining the integrity of linker histone binding is micrococcal nuclease digestion (*38*, *52*, *53*). Whereas nucleosomes strongly protect ~145 bp of DNA from digestion, linker histone binding leads to stable protection of an additional 20 bp of linker DNA. Figure 3B shows the results of micrococcal nuclease digestion of our purified 208-12 nucleosomal array and chromatin preparations. Both the nucleosomal arrays and chromatin exhibited kinetic pauses at ~165 and ~145 bp. For the nucleosomal arrays, the total amount of 165 bp band decreased while the amount of the 145 bp band increased over the time course of the experiment. Small amounts of subnucleosomal bands also were apparent in the last time point. In contrast, the purified 208-12 chromatin displayed a pronounced kinetic "chromatosome" stop (*38*, *48*, *52*−*55*) throughout the entire digestion time course (Figure 3B). The 208-12 chromatin also exhibited a significant decrease in the cleavage rate at earlier nuclease digestion points (data not shown). These results indicate that purified 208-12 chromatin possesses all of the classical features observed upon micrococcal nuclease digestion of native chromatin.

The molecular basis of the chromatosome stop is believed to arise from a linker histone-dependent protection of nucleosomal DNA (*3*, *4*, *9*), and is correlated with a constraint in linker DNA path that produces a three-dimensional "zigzag" arrangement of nucleosomes and linker DNA (*11*, *12*). To visualize the linker DNA conformation of reconstituted 208-12 chromatin, as well as to directly compare its morphology with native chromatin, we examined unfixed and unstained reconstitutes using electron cryomicroscopy (ECM) (*33*, *56*). This technique has recently proven very useful for studying the three-dimensional conformation of chromatin and nucleosomes in a more solution-like environment than other microscopic approaches (*33*, *34*, *56*−*58*). Representative ECM images of 208-12 nucleosomal arrays and 208-12 chromatin vitrified in 5 mM NaCl, 10 mM Tris, and 0.2 mM EDTA are shown in Figure 4. In the absence of H5, 208-12 nucleosomal arrays were present in an extended conformation (Figure 4A). In contrast, the linker histone-containing 208-12 nucleosomal arrays were significantly more compact (Figure 4B), consistent with the solution-state biophysical data (Figure 2B and Table 2). In addition, the ECM images showed clearly that the entering and exiting linker DNA was constrained in the 208-12 chromatin, effectively compacting the arrays (arrows in Figure 4B). Typically, the linker DNA segments were now closely apposed to each other, as also has been observed for reconstituted mononucleosomes (*57*) and in several native chromatins (*58*). The final question addressed was whether the morphology of the in vitro-assembled 208-12 chromatin differed from that of native chromatin. To enable the overall conformation to be seen more clearly, 208-6 chromatin (Figure 4C) and purified chicken erythrocyte chromatin of the same length range (Figure 4D) were examined by ECM. The native and reconstituted 208-6 chromatin samples were morphologically indistinguishable, both frequently appearing in star-like zigzag conformations. Also, in both cases, the constrained stem motif of the linker DNA segments (*33*, *57*, *58*) was common (arrows in Figure 4C,D).

Taken together, the data presented thus far indicate that we have successfully assembled and purified milligram quantities of 208-12 chromatin that possesses native linker histone stoichiometry and appears morphologically indistinguishable from native chromatin under low-salt conditions. We next used the purified 208-12 chromatin preparations for solution-state biophysical studies of salt-dependent chromatin folding and oligomerization.

Reversible Oligomerization in NaCl and $MgCl_2$. Previous work has shown that linker histone-containing nucleosomal arrays oligomerize in both monovalent and divalent salts (*59*, *60*), while nucleosomal arrays lacking linker histones oligomerize only in divalent salts (*36*, *61*). There are several reasons for studying oligomerization. First, from a practical point of view, it is necessary to precisely determine the salt dependence of oligomerization to define the range of salt concentrations in which chromatin folding can be studied (*17*, *19*, *20*). In addition, the previously defined oligomerization behavior of native chromatin provides another benchmark for successful H5 reconstitution. Finally, there is evidence suggesting that in vitro oligomerization of small chromatin fragments may be related to the long-range condensation phenomena found in chromosomal fibers in vivo (*5*, *36*). The oligomerization profiles of purified 208-12 nucleosomal arrays and chromatin in NaCl and $MgCl_2$ are shown in Figure 5. These experiments were carried out using the differential centrifugation approach developed previously (*17*, *36*). Consistent with previous results (*36*, *59*), 208-12 nucleosomal arrays did not oligomerize in NaCl. In contrast, purified 208-12 chromatin was 50% oligomerized in ~120 mM NaCl. In $MgCl_2$, half-maximal oligomerization of purified 208-12 nucleosomal arrays and chromatin occurred at ~3.25 and ~1.5 mM $MgCl_2$, respectively. The oligomerization profiles shown in Figure 5 have defined the optimal NaCl and $MgCl_2$ concentrations for studying salt-dependent chromatin folding. In addition, these data provide further evidence that the properties of purified 208-12 chromatin are indistinguishable from those of native chromatin.

Salt-Dependent Folding of Purified 208-12 Nucleosomal Arrays and Chromatin. It is well documented that 208-12 nucleosomal arrays in salt solutions are in equilibrium between a 29S unfolded conformation, a 40S folding intermediate, and an ~55S maximally folded state (*5*, *15*−*17*, *19*, *20*). However, the extensively folded structures formed by nucleosomal arrays in the absence of linker histones are not stable (*5*, *17*). We therefore addressed two key mechanistic questions that have been the subject of widespread speculation but presently remain unresolved (*5*, *14*, *37*). Does H5 binding alter the intrinsic 29S ↔ 40S ↔ 55S folding pathway of 208-12 nucleosomal arrays? Relative to saturated arrays, what are the folding properties of chromatin consisting of slightly substoichiometric amounts of core histone octamers and linker histones? To answer these questions, sedimentation velocity studies of purified 208-12 nucleosomal arrays and chromatin were performed in both NaCl and $MgCl_2$. As demonstrated previously (*15*,

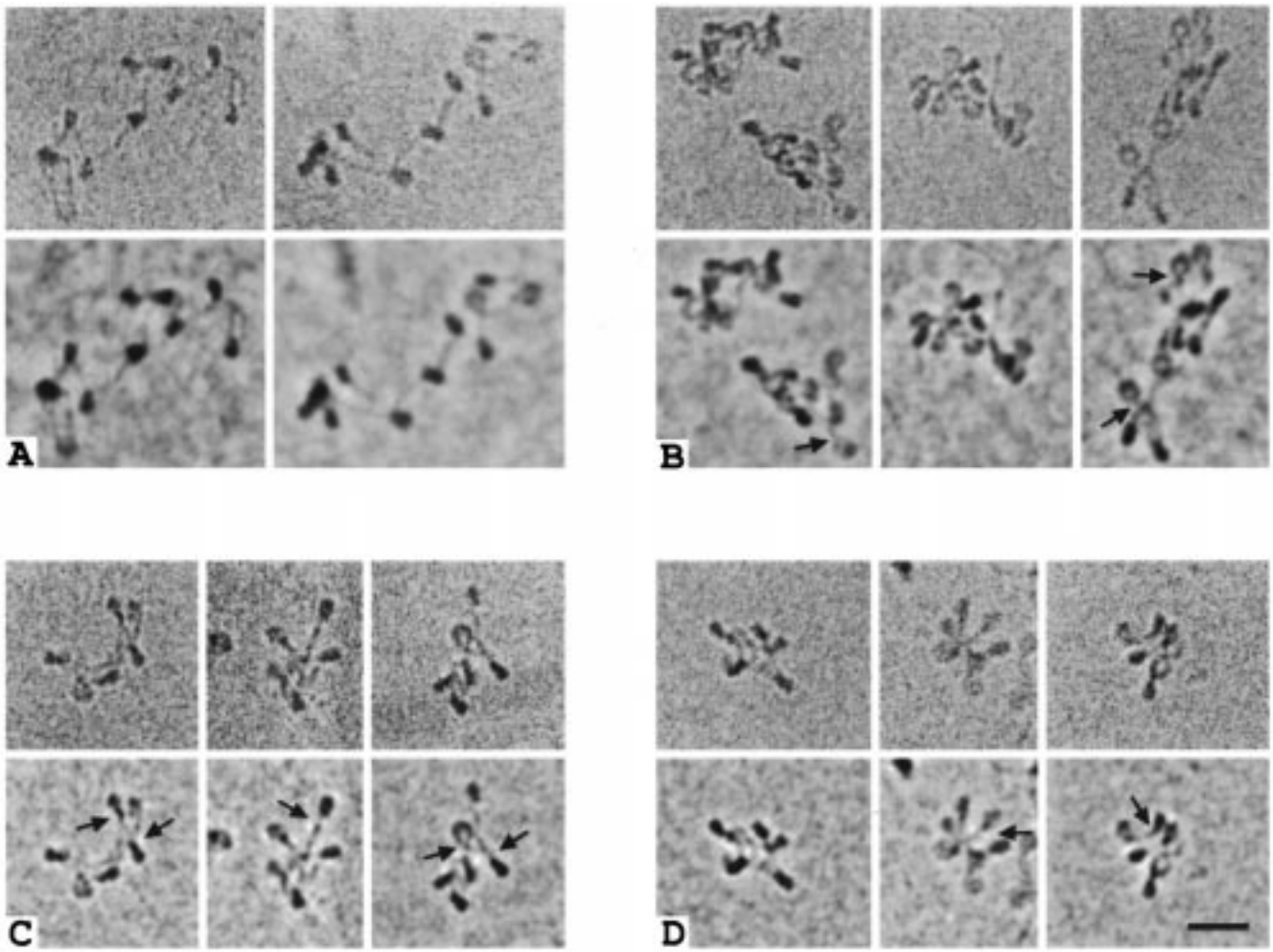

FIGURE 4: Electron cryomicroscopy of reconstituted and native chromatin. In all cases, unprocessed images are shown above the CTF-corrected images. CTF correction reduces the defocus effect, and allows clearer visualization of nucleosomes and linker DNA (see Experimental Procedures). Since the arrays were freely suspended in buffer until the moment of cryoimmobilization, the images provide a "snapshot" of the dynamic solution conformation, and three-dimensional information can be retrieved from the stereopairs. (A) 208-12 nucleosomal arrays lacking histone H5 exhibit a loose "beads-on-a-string" conformation with nucleosomes well separated and linker DNA unconstrained. Each array contains 12 octamers, although this is evident only in stereo (not shown here). (B) 208-12 chromatin has a more compact conformation due to the strongly constrained linker DNA segments at the nucleosome entry and/or exit sites. As a consequence, many nucleosomes are overlapped or superpositioned in single projection images. Arrows point to the "stem" motif formed by the constrained entering and exiting linker DNA. (C) Individual nucleosomes and linker DNA are seen more clearly in the 208-6 chromatin. The zigzag architecture produces a starlike conformation in some orientations, and the linker DNA stem motif is common (arrows). For this experiment, 208-6 chromatin was reconstituted as described previously (*38*, *39*). (D) Native chicken erythrocyte chromatin ($N = 5-7$) adopts a conformation that is indistinguishable from the 208-6 chromatin. Again, a starlike conformation is frequent, and the constrained linker DNA stem motif is common (arrows). The scale is 30 nm.

17, *19*, *20*), analysis of the data by the method of van Holde and Weischet (*28*) provides a very accurate indication of the extent of folding of all species in the sample under a given set of solution conditions. In this case, ~60−70% of the 208-12 nucleosomal array and chromatin preparations utilized were saturated while ~30−40% were slightly subsaturated (Figures 1 and 3). Thus, in the resulting sedimentation coefficient distribution plots shown in Figures 6 and 7, boundary fractions of 0.45−1.0 will yield information about the saturated arrays while boundary fractions of 0.05−0.4 will describe the behavior of the subsaturated species. Ultimately, the sedimentation velocity experiments have made it possible for the first time to simultaneously determine folding behavior of saturated and slightly subsaturated chromatin under identical solution conditions.

The results obtained in 20 and 80 mM NaCl are shown in Figure 6. The saturated nucleosomal array fraction sedimented as a heterogeneous population of 30S−37S species in 20 mM NaCl (Figure 6A). Strikingly, the saturated 208-12 chromatin fraction in 20 mM NaCl sedimented as a nearly homogeneous 40S species. The sedimentation coefficients of the subsaturated nucleosomal array and chromatin fractions in 20 mM NaCl ranged from 27S to 30S and 36S to 39S, respectively. In 80 mM NaCl, the sedimentation coefficients of 208-12 nucleosomal arrays increased by 2S−3S across the entire distribution relative to their profiles in 20 mM NaCl (compare panels A and B of Figure 6), and both the saturated and subsaturated nucleosomal array fractions remained noticeably heterogeneous. The saturated and subsaturated populations of 208-12 chromatin both sedimented substantially faster in 80 mM NaCl than the corresponding nucleosomal array population (Figure 6B). Furthermore, the homogeneous 40S chromatin species present in 20 mM NaCl was converted to a heterogeneous population of more extensively folded 45S−55S structures in 80 mM NaCl, while the subsaturated fraction increased by only 3S−

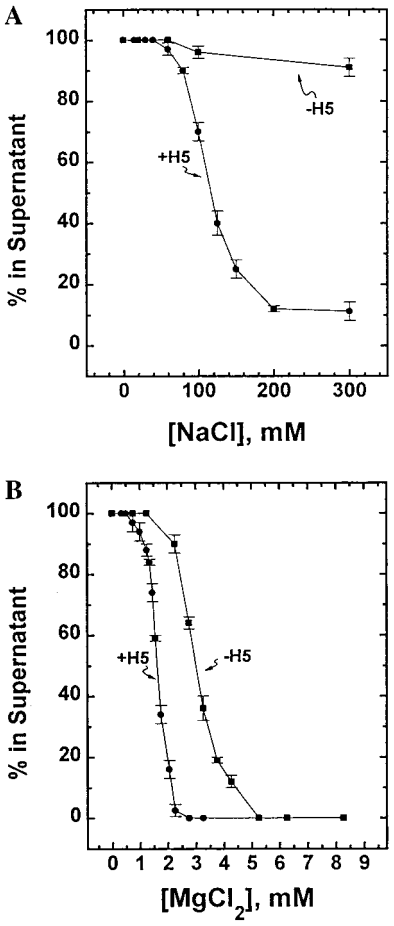

FIGURE 5: Salt-dependent oligomerization of purified 208-12 nucleosomal arrays and chromatin in NaCl (A) and $MgCl_2$ (B). Shown is the percentage of the nucleosomal array (■) and chromatin (●) samples that remained in the supernatant after centrifugation for 10 min at 16000*g* in an Eppendorf microcentrifuge. Each data point represents the mean ± the standard deviation of at least four determinations.

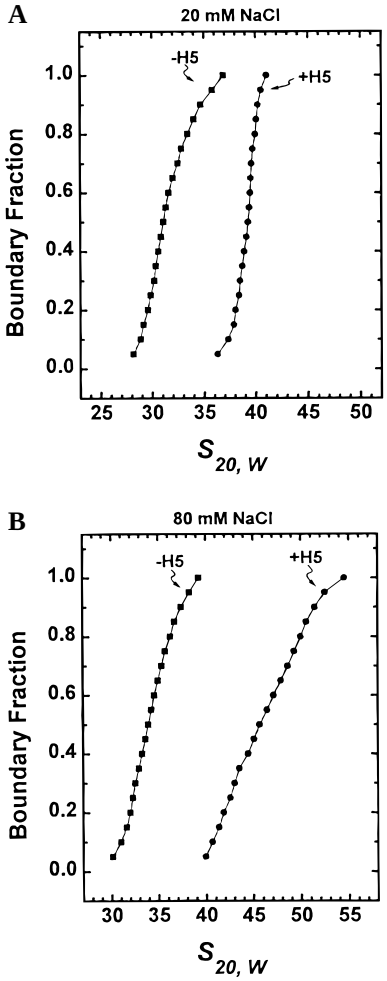

FIGURE 6: Sedimentation velocity analysis of purified 208-12 nucleosomal arrays and chromatin in NaCl. (A) Sedimentation coefficient distribution plots obtained for nucleosomal arrays (■) and chromatin (●) in 20 mM NaCl. (B) Sedimentation coefficient distribution plots obtained for nucleosomal arrays (■) and chromatin (●) in 80 mM NaCl. Due to the fact that ~10% of the chromatin sample was supersaturated (Figure 3), the top 10% of the boundaries were not included in the analysis.

4S across the distribution under these ionic conditions (Figure 6B). Thus, saturated 208-12 chromatin did not form a stable, 55S species in NaCl prior to the onset of oligomerization, consistent with previous studies of native chromatin (*62*). Together, the data in Figure 6 establish clearly that histone H5 binding markedly drives the equilibrium toward the more extensively folded states of saturated and subsaturated 208-12 chromatin in both 20 and 80 mM NaCl, although a stable 55S conformation was not achieved under these conditions. They further indicate that the global stability of 208-12 chromatin that is even slightly deficient in either histone octamers or histone H5 is reduced significantly relative to that of saturated 208-12 chromatin under the same salt conditions.

Several additional key results were obtained when the sedimentation studies were repeated in $MgCl_2$. The pronounced stabilizing effect of H5 on Na^+-dependent chromatin folding (Figure 6) also was present in $MgCl_2$ (Figure 7A,B). However, at the highest Mg^{2+} concentration that could be studied prior to bulk oligomerization (0.65 mM), 208-12 chromatin was substantially more compact in $MgCl_2$ than in NaCl (compare Figures 6B and 7B). Of particular significance, the saturated 208-12 chromatin fraction sedimented as a nearly homogeneous ~57S species in 0.65 mM $MgCl_2$, with the onset of oligomerization also evident at the very top of the distribution plot under these salt conditions (Figure 7B). It cannot be discerned whether the small degree of sedimentation coefficient heterogeneity of the saturated chromatin fraction in 0.65 mM $MgCl_2$ reflects the presence of slight conformational heterogeneity or results from the inherent limitations in the analysis method (*63*). The sedimentation data shown in Figure 7B provide the first demonstration that the fraction of 208-12 chromatin containing stoichiometric amounts of histone octamers and linker histones can be completely stabilized in the maximally condensed 55S structure. To verify these results using an entirely different experimental approach, we measured the R_e of purified 208-12 nucleosomal arrays and chromatin in agarose multigels containing 0.65 mM $MgCl_2$. Under these salt conditions, the R_e of purified 208-12 nucleosomal arrays was 24.0 ± 1.5 nm while that of the 208-12 chromatin was 15.5 ± 1.0 nm (Figure 7B inset). Because the 55S conformation of a 208-12 nucleosomal array is approaching a globular shape (*15*), the R_e determined under these conditions gives a reasonable measure of the actual radius of maximally folded 208-12 chromatin. Thus, the quantitative gel data demonstrate directly that saturated 208-12

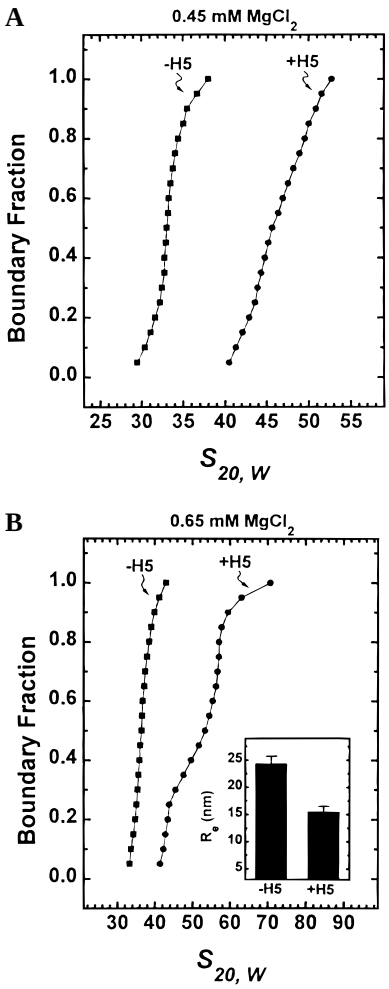

FIGURE 7: Sedimentation velocity analysis of purified 208-12 nucleosomal arrays and chromatin in $MgCl_2$. (A) Sedimentation coefficient distribution plots obtained for nucleosomal arrays (■) and chromatin (●) in 0.45 mM $MgCl_2$. (B) Sedimentation coefficient distribution plots obtained for nucleosomal arrays (■) and chromatin (●) in 0.65 mM $MgCl_2$. Due to the fact that ~10% of the chromatin sample was supersaturated, the top 10% of the boundaries were not included in the analysis. The inset shows the R_e values of the purified nucleosomal array and chromatin samples as determined from agarose multigels containing 0.65 mM free Mg^{2+} (see Experimental Procedures). Each R_e value represents the mean ± standard deviation of seven determinations.

chromatin in 0.65 mM $MgCl_2$ folds into an extensively condensed ~30 nm diameter conformation. Interestingly, the subsaturated chromatin fraction sedimented as a heterogeneous population of 40S−54S structures in 0.65 mM $MgCl_2$, establishing unequivocally that 208-12 chromatin that is even slightly depleted in histone octamers and linker histones is incapable of maintaining a stable, maximally folded conformation.

Finally, to determine the maximum extent of folding possible in the absence of histone H5, sedimentation velocity analyses of 208-12 nucleosomal arrays in 2 mM $MgCl_2$ were performed. As reported previously (*17*, *19*, *20*, *36*), a very broad distribution of sedimentation coefficients ranging from 29S to 55S with a characteristic discontinuity in the profile at ~40S was observed (Figure 8). These data provide a clear indication of the intrinsic 29S ↔ 40S ↔ 55S folding pathway of 208-12 nucleosomal arrays. Given the composition of the purified nucleosomal arrays used for these experiments (Figure 1), it is retrospectively apparent that the discontinuity

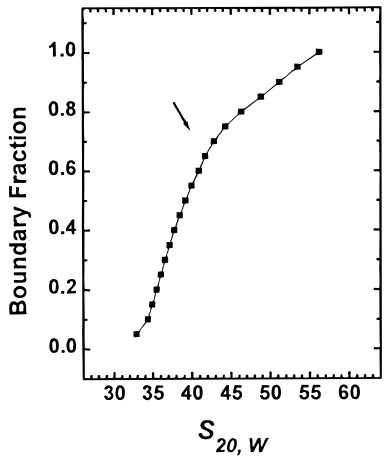

FIGURE 8: Sedimentation velocity analysis of purified 208-12 nucleosomal arrays in 2 mM $MgCl_2$. The arrow indicates the discontinuity in the sedimentation coefficient distribution plot at ~40S.

in the distribution plot arises primarily from the fact that the saturated nucleosomal array fraction sediments between 40S and 55S in 2 mM $MgCl_2$, while the subsaturated fraction lacking even a single histone octamer sediments between 30S and 40S. These data confirm that a single gap in the 12-mer nucleosomal array is sufficient to disrupt formation of the maximally folded 55S state (*17*). Also, the fact that subsaturated 12-mer nucleosomal arrays can form the intermediate 40S conformation but not the 55S state is consistent with a mechanism in which the close approach of a stretch of five to seven adjacent nucleosomes is the requisite first step in higher-order chromatin folding. These results ultimately show that given sufficient charge neutralization, nucleosomal arrays lacking linker histones can form a maximally folded 55S structure that is as equally compact as the maximally folded state stabilized by linker histones, although only ~5% of the total nucleosomal array population exists in this conformational state under these salt conditions.

DISCUSSION

In the absence of other chromatin-associated proteins, nucleosomal arrays are capable of forming extensively folded structures through a mechanism that is dependent on divalent cations (*17*) and multiple distinct functions of the core histone N termini (*16*, *18*−*20*, *23*). However, despite possessing the intrinsic ability to condense through the action of the core histone N termini, the folded states of nucleosomal arrays are unstable (*15*−*17*). Stable 30 nm folded chromatin fibers are observed only when linker histones are components of the nucleosomal array (*14*, *64*). Thus, it now seems likely that there is considerable, albeit poorly understood, structural and functional interplay between the linker histones and core histone N termini during higher-order chromatin folding. In this regard, a key unsolved issue (*5*, *14*) is whether the actions of linker histones cause chromatin to fold through a pathway entirely different than that exhibited by nucleosomal arrays lacking linker histones, or whether linker histones function without fundamentally altering the intrinsic folding pathway of nucleosomal arrays.

Previous attempts to delineate the folding pathways of linker histone-containing nucleosomal arrays were performed with chromatin preparations that were heterogeneous in size,

and hence only yielded information about the average extent of sample folding (*37*, *44*, *48*, *53*, *54*, *65*, *66*). Unfortunately, due to the complexity of the condensation process, average chromatin folding data are very difficult to definitively interpret (*31*). In addition, it is also difficult to selectively manipulate the histone octamer and linker histone content of heterogeneous chromatin samples, which ultimately is necessary for subsequent investigations of the complex functions of the core histone N termini and linker histones during chromatin folding. These problems in principle can be circumvented through the use of the length-defined 5S nucleosomal array model systems developed by Simpson et al. (*24*). An additional advantage of these systems is that their intrinsic folding pathway has been characterized extensively (*15*−*21*, *23*). However, a number of technical problems had to be solved before the 5S nucleosomal arrays could prove useful for studies of linker histone effects on chromatin folding. Specifically, the model systems must be assembled such that the proper stoichiometry of both core histone octamers and linker histone is achieved; it must be documented that the linker histones are bound to the nucleosomal arrays in the same manner as in native chromatin, and it must be possible to assay for the extent of folding of all species in the sample rather than just the average extent of folding. In this work, each of these criteria has been realized. Novel purification protocols applied after both nucleosomal array assembly and histone H5 binding have routinely yielded samples in which ≥60% of the 208-12 DNA templates contain 12 histone octamers and physiological levels of histone H5 (Figures 1−3 and Tables 1 and 2). Nuclease digestion experiments with the purified 208-12 chromatin have revealed a classical ∼165 bp chromatosome stop (Figure 3B); electron cryomicroscopy has demonstrated that the morphology of purified 208-12 chromatin and endogenous chicken erythrocyte chromatin are indistinguishable (Figure 4; *58*), and the salt-dependent oligomerization properties of native chromatin and 208-12 chromatin are essentially identical (Figure 5; *59*−*61*). In terms of the folding assay, sedimentation velocity experiments analyzed by the method of van Holde and Weischet (*28*) yield the compaction state of all species in solution, both when the chromatin is extended under low-salt conditions (Figures 1−3) and during salt-dependent formation of higher-order folded structures (Figures 6−8). Together, these results demonstrate that purified 208-12 chromatin provides a legitimate, powerful model system for studying the mechanisms of linker histone action during chromatin folding.

Our initial investigation of the salt-dependent compaction of 208-12 chromatin has demonstrated that histone H5 stabilizes higher-order chromatin folding without altering the fundamental folding pathway observed when linker histones are absent. The stabilizing effects of linker histones are apparent throughout the entire folding process. At NaCl and $MgCl_2$ concentrations that are not sufficient to promote maximal folding, purified 208-12 chromatin is always substantially more compacted than the parent nucleosomal arrays under the same conditions (Figures 6 and 7). Perhaps most importantly, saturated 208-12 chromatin in 0.65 $MgCl_2$ folds into a highly homogeneous ∼57S conformation having an effective diameter of ∼31 nm (Figure 7B). This is in distinct contrast to the results from nucleosomal arrays lacking linker histones, where a maximum of ∼5% of the saturated sample exists in the ∼55S state under optimal Mg^{2+} conditions. Several lines of evidence support the conclusion that the intrinsic 29S ↔ 40S ↔ 55S folding pathway of 208-12 nucleosomal arrays is preserved during folding of 208-12 chromatin. For example, saturated 208-12 chromatin sediments as a homogeneous 40S species during the initial stages of folding in 20 mM NaCl (Figure 6A) and as an essentially homogeneous ∼57S species at the termination of folding in 0.65 mM $MgCl_2$ (Figure 7B). In addition, saturated 208-12 chromatin in 0.45 $MgCl_2$, subsaturated 208-12 chromatin in 0.65 mM $MgCl_2$, and saturated 208-12 nucleosomal arrays in 2 mM $MgCl_2$ each exhibited essentially identical sedimentation coefficient distribution profiles ranging from ∼40S to 55S. These data show that the folding pathway of 208-12 nucleosomal arrays, both in the absence and in the presence of linker histones, involves the initial formation of a defined ∼40S folding intermediate followed by further compaction into a maximally folded ∼55S conformation. This in turn suggests that the functions of the core histone N termini in chromatin folding remain unaltered by the presence of bound histone H5. The sedimentation results are in agreement with recent atomic force (*12*) and electron cryomicroscopy (*33*, *58*) studies of native chromatin in NaCl and $MgCl_2$. In 20−80 mM NaCl, both microscopic approaches show that adjacent, but not consecutive, nucleosomes initially become closer in three-dimensional space. The atomic force microscopy studies further demonstrate that an even more condensed structure forms in $MgCl_2$. These results ultimately suggest that native chromatin initially forms a defined intermediate having the same properties as the 40S state of 208-12 nucleosomal arrays prior to formation of the maximally folded 30 nm fiber.

In light of the many recent advances made toward understanding the macromolecular determinants of chromatin folding, we envision the following functions for the core histone N termini, linker histones, and cations during chromatin compaction. It is well established that the free energy required to form stable 30 nm chromatin fibers is contributed almost entirely by DNA charge neutralization (*62*, *67*, *68*). Both inorganic cations and linker histones clearly are required to achieve complete stability; chromatin in TE remains extended (Figures 3A and 4), while nucleosomal arrays lacking linker histones exist as a heterogeneous population of partially folded structures in salts (Figures 6−8; *15*, *16*). The stabilizing effect of linker histones appears to be mediated by the large positive surface charge density in the linker histone C and N termini (*53*, *66*). In contrast, the core histone N termini perform separate functions and act through different mechanisms. These domains clearly make no substantive contribution to stability, as evidenced by the broad distribution of partially folded structures observed in the absence of linker histones. At the same time, the N termini are absolutely required for higher-order folding of both nucleosomal arrays (*16*, *18*, *19*, *23*) and chromatin (*54*). We believe the most likely explanation for these results is that the core histone N termini are required to specify both the short-range and long-range nucleosome−nucleosome interactions in cis that lead to formation of intermediate and maximally folded conformational states of nucleosomal arrays and chromatin. Interestingly, segregation of the molecular interactions that provide specificity and stability

is a common theme in many other biological phenomena, including dsDNA structure (*69*) and protein folding (*70*). Finally, it should be noted that linker histones also provide an additional function that stems from the molecular consequences of the constraint of the entering and exiting linker DNA. Electron cryomicroscopy studies of mononucleosomes (*57*), as well as ECM of native chromatin fragments (*33*) and reconstituted 208-12 chromatin model systems (*58*), have shown that the linker DNA segments that enter and exit each nucleosome form a unique apposed structural motif that is not present in the absence of linker histones. This motif clearly influences the specific structure of the chromatin fiber during subsequent compaction in salt (*58*). Thus, linker histones both stabilize chromatin folding and dictate the specific structure of the higher-order folded states of chromatin but do not appear to directly contribute to the internucleosomal interactions required for chromatin folding.

ACKNOWLEDGMENT

We thank V. Schirf for technical support and K. van Holde for advice on linker histone reassociation. We also thank C. Tse for critically reading the manuscript.

REFERENCES

1. Belmont, A. S., and Bruce, K. (1994) *J. Cell Biol. 127*, 287−302.
2. Li, G., Sudlow, G., and Belmont A. S. (1998) *J. Cell Biol. 140*, 975−989.
3. van Holde, K. E. (1988) *Chromatin*, Springer-Verlag, New York.
4. Wolffe, A. P. (1995) *Chromatin: Structure & Function*, 2nd ed., Academic Press, New York.
5. Fletcher, T. M., and Hansen, J. C. (1996) *Crit. Rev. Eukaryotic Gene Expression 6*, 149−188.
6. Arents, G., and Moudrianakis E. N. (1993) *Proc. Natl. Acad. Sci. U.S.A. 90*, 10489−10493.
7. Arents, G., and Moudrianakis E. N. (1995) *Proc. Natl. Acad. Sci. U.S.A. 92*, 11170−11174.
8. Luger, K., Mader, A. W., Richmond, R. K., Sargent, D. F., and Richmond, T. J. (1997) *Nature 389*, 251−260.
9. Widom, J. (1989) *Annu. Rev. Biophys. Biophys. Chem. 18*, 365−395.
10. Hansen, J. C. (1997) *Chemtracts: Biochem. Mol. Biol. 11*, 56−69.
11. Woodcock, C. L., and Horowitz, R. A. (1995) *Trends Cell Biol. 5*, 272−277.
12. Zlatanova, J., Leuba, S. H., and van Holde K. E. (1998) *Biophys. J. 74*, 2554−2566.
13. Ramakrishnan, V. (1998) *Crit. Rev. Eukaryotic Gene Expression 7*, 215−230.
14. Thoma, F., Koller, T., and Klug, A. (1979) *J. Cell Biol. 83*, 402−427.
15. Hansen, J. C., Ausio, J., Stanik, V. H., and van Holde, K. E. (1989) *Biochemistry 28*, 9129−9136.
16. Garcia-Ramirez, M., Dong, F., and Ausio, J. (1992) *J. Biol. Chem. 267*, 19587−19595.
17. Schwarz, P. M., and Hansen, J. C. (1994) *J. Biol. Chem. 269*, 16284−16289.
18. Fletcher, T. M., and Hansen, J. C. (1995) *J. Biol. Chem. 270*, 25359−25362.
19. Tse, C., and Hansen, J. C. (1997) *Biochemistry 36*, 11381−11388.
20. Tse, C., Sera, T., Wolffe, A. P., and Hansen, J. C. (1998) *Mol. Cell. Biol. 18*, 4629−4638.
21. Garcia-Ramirez, M., Rocchini, C., and Ausio, J. (1995) *J. Biol. Chem. 270*, 17923−17928.
22. Krajewski, W. A., and Ausio, J. (1996) *Biochem. J. 316*, 395−400.
23. Moore, S. C., and Ausio, J. (1997) *Biochem. Biophys. Res. Commun. 230*, 136−139.
24. Simpson, R. T., Thoma, F., and Brubaker, J. M. (1985) *Cell 42*, 799−808.
25. Georgel, P., Demeler, B., Terpening, C., Paule, M. R., and van Holde, K. E. (1993) *J. Biol. Chem. 268*, 1947−1954.
26. Garcia-Ramirez, M., Leuba, S., and Ausio, J. (1990) *Protein Expression Purif. 1*, 40−44.
27. Hansen, J. C., and Lohr, D. (1993) *J. Biol. Chem. 268*, 5840−5848.
28. van Holde, K. E., and Weischet, W. O. (1978) *Biopolymers 17*, 1387−1403.
29. Fletcher, T. M., Krishnan, U., Serwer, P., and Hansen, J. C. (1994) *Biochemistry 33*, 2226−2233.
30. Fletcher, T. M., Serwer, P., and Hansen, J. C. (1994) *Biochemistry 33*, 10859−10863.
31. Hansen, J. C., Kreider, I. K., Demeler, B., and Fletcher, T. M. (1997) *Methods 12*, 62−72.
32. Griess, G. A., Moreno, E. T., Easom, R., and Serwer, P. (1989) *Biopolymers 28*, 1475−1484.
33. Bednar, J., Horowitz, R. A., Dubochet, J., and Woodcock, C. L. (1995) *J. Cell Biol. 131*, 1365−1376.
34. Woodcock, C. L., and Horowitz, R. A. (1997) *Methods 12*, 84−95.
35. Carruthers, L. M., Tse, C., Walker, K. P., III, and Hansen, J. C. (1998) *Methods Enzymol*. (in press).
36. Schwarz, P. M., Felthauser, A., Fletcher, T. M., and Hansen, J. C. (1996) *Biochemistry 35*, 4009−4015.
37. Graziano, V., Gerchman, S. E., and Ramakrishnan, V. (1988) *J. Mol. Biol. 203*, 997−1007.
38. Meersseman, G., Pennings, S., and Bradbury, E. M. (1991) *J. Mol. Biol. 220*, 89−100.
39. Howe, L., Iskandar, M., and Ausio, J. (1998) *J. Biol. Chem. 273*, 11625−11629.
40. Hayes, J. J., and Wolffe, A. P. (1993) *Proc. Natl. Acad. Sci. U.S.A. 90*, 6415−6419.
41. An, W., Leuba, S., van Holde, K., and Zlatanova, J. (1998) *Proc. Natl. Acad. Sci. U.S.A. 95*, 3396−3401.
42. Guschin, D., Chandler, S., and Wolffe, A. P. (1998) *Biochemistry 37*, 8629−8636.
43. Drew, H. R., and McCall, M. J. (1987) *J. Mol. Biol. 197*, 485−511.
44. Allan, A. D., Staynov, D. Z., and Gould, H. (1980) *Proc. Natl. Acad. Sci. U.S.A. 77*, 885−889.
45. Thoma, F., and Koller, T. (1981) *J. Mol. Biol. 149*, 709−733.
46. Thoma, F., Losa, R., and Koller, T. (1983) *J. Mol. Biol. 167*, 619−640.
47. Kaplan, L. J., Gauer, R., Morrison, E., Langan, T. A., and Fasman, G. D. (1983) *J. Biol. Chem. 259*, 8777−8785.
48. Allan, J., Cowling, G. J., Harborne, N., Cattini, P., Craigie, R., and Gould, H. J. (1981) *J. Cell Biol. 90*, 279−288.
49. Ruiz-Carrillo, A., Affolter, M., and Renaud, J. (1983) *J. Mol. Biol. 170*, 843−859.
50. Krieg, P. A., Robins, A. J., D'Andrea, R., and Wells, J. R. E. (1983) *Nucleic Acid Res. 11*, 619−627.
51. Bates, D. L., and Thomas, J. O. (1981) *Nucleic Acid Res. 9*, 5883−5894.
52. Simpson, R. T. (1978) *Biochemistry 17*, 5524−5531.
53. Allan, J., Hartman, P. G., Crane-Robinson, C., and Aviles, F. X. (1980) *Nature 288*, 675−679.
54. Allan, J., Harborne, N., Rau, D. C., and Gould, H. (1982) *J. Cell Biol. 93*, 285−297.
55. Staynov, D. Z., and Crane-Robinson, C. (1988) *EMBO J. 7*, 3685−3691.
56. Dubochet, J., Adrian, M., Chang, J. J., Homo, J. C., Lepault, J., McDowall, A. W., and Schultz, P. (1988) *Q. Rev. Biophys. 21*, 129−228.
57. Hamiche, A., Schultz, P., Ramakrishnan, V., Oudet, P., and Prunell, A. (1996) *J. Mol. Biol. 257*, 30−42.
58. Bednar, J., Horowitz, R. A., Grigoryev, S. A., Carruthers, L. M., Hansen, J. C., Koster, A. J., and Woodcock, C. L. (1998) *Proc. Natl. Acad. Sci. U.S.A.* (submitted for publication).

59. Ausio, J., Borochov, N., Seger, D., and Eisenberg, H. (1984) *J. Mol. Biol. 177*, 373−398.
60. Jin, Y.-J., and Cole, R. D. (1986) *J. Biol. Chem. 261*, 15805−15812.
61. Ausio, J., Sasi, R., and Fasman, G. D. (1986) *Biochemistry 25*, 1981−1988.
62. Widom, J. (1986) *J. Mol. Biol. 190*, 411−424.
63. Demeler, B., Saber, H., and Hansen, J. C. (1997) *Biophys. J. 72*, 397−407.
64. Thoma, F., and Koller, T. (1977) *Cell 12*, 101−107.
65. Butler, P. J. G., and Thomas, J. O. (1980) *J. Mol. Biol. 140*, 505−529.
66. Allan, J., Mitchell, T., Harborne, N., Bohm, L., and Crane-Robinson, C. (1986) *J. Mol. Biol. 187*, 591−601.
67. Clark, D. J., and Kimura, T. (1990) *J. Mol. Biol. 211*, 883−896.
68. Subirana, J. A. (1992) *FEBS Lett. 302*, 105−107.
69. Rose, G. D., and Creamer, T. P. (1994) *Proteins: Struct., Funct., Genet. 19*, 1−3.
70. Spolar, R. S., and Record, M. T., Jr. (1994) *Science 263*, 777−784.

BI981684E